


Evidence for short-range magnetic order in the nematic phase of FeSe from anisotropic in-plane magnetostriction and susceptibility measurements

Mingquan He,¹ Liran Wang,¹ Frédéric Hardy,¹ Liping Xu,^{1,2} Thomas Wolf,¹ Peter Adelman,¹ and Christoph Meingast^{1,*}

¹*Institute for Solid State Physics, Karlsruhe Institute of Technology, Karlsruhe 76021, Germany*

²*Key Laboratory of Polar Materials and Devices, Ministry of Education, Department of Electronic Engineering, East China Normal University, Shanghai 200241, China*

 (Received 12 September 2017; revised manuscript received 15 February 2018; published 19 March 2018)

The nature of the nematic state in FeSe remains one of the major unsolved mysteries in Fe-based superconductors. Both spin and orbital physics have been invoked to explain the origin of this phase. Here we present experimental evidence for frustrated, short-range magnetic order, as suggested by several recent theoretical works, in the nematic state of FeSe. We use a combination of magnetostriction, susceptibility, and resistivity measurements to probe the in-plane anisotropies of the nematic state and its associated fluctuations. Despite the absence of long-range magnetic order in FeSe, we observe a sizable in-plane magnetic susceptibility anisotropy, which is responsible for the field-induced in-plane distortion inferred from magnetostriction measurements. Further we demonstrate that all three anisotropies in FeSe are very similar to those of BaFe₂As₂, which strongly suggests that the nematic phase in FeSe is also of magnetic origin.

DOI: [10.1103/PhysRevB.97.104107](https://doi.org/10.1103/PhysRevB.97.104107)

I. INTRODUCTION

Magnetism appears to be the universal driving force for high-temperature superconductivity in, e.g., cuprates and Fe-based compounds [1,2]. However, this scenario has been challenged by the structurally simple iron chalcogenide FeSe. Unlike iron-pnictide compounds, long-range magnetic order is absent in stoichiometric FeSe at ambient pressure, although it does undergo a similar structural transition to an electronic nematic state [3–6]. The microscopic nature of this state of reduced rotational symmetry, from which superconductivity emerges, remains enigmatic, and both spin [7–10] and orbital [11–14] degrees of freedom have been intensively discussed. At first glance, the absence of static magnetism seems to discredit the spin-nematic scenario and favors an orbital order [15–20]. However, recent theoretical proposals indicate that the magnetic interactions in FeSe are highly frustrated, suppressing magnetic (but not nematic) order [21–23]. Experimentally, this interpretation is supported by the observation of low-energy spin fluctuations along the $(\pi, 0)$ wave vector below the nematic transition at T_S [24–26]. To date, the nematic phase of FeSe has been studied by means of elastic modulus [15,27,28], transport [6,29], neutron scattering [24–26,30], and Raman spectroscopies [31,32], angle-resolved photoemission spectroscopy [6], and NMR measurements [15–17]. Direct measurements of the in-plane magnetic anisotropy like in BaFe₂As₂, which allows us to disentangle between magnetic and orbital orders [33], are, however, still lacking.

In this paper, the anisotropic magnetic response of FeSe is studied using a combination of magnetostriction, magnetic susceptibility, and resistivity measurements on FeSe single

crystals in order to unravel the nature of the nematic state. Magnetization measurements on uniaxially strained FeSe clearly show a substantial in-plane magnetic susceptibility anisotropy developing within the nematic phase. This anisotropy agrees well with our magnetostriction measurements, which provide an indirect measure of the susceptibility anisotropy. Surprisingly, the temperature dependence of both the susceptibility and transport anisotropies are extremely similar to that of long-range magnetically ordered BaFe₂As₂, although the signs of both quantities are reversed. It was theoretically demonstrated that orbital order alone is insufficient to produce a sizable susceptibility anisotropy [33] and that magnetic order and spin-orbit coupling are essential. Here using this same reasoning, we argue that our data therefore provide strong evidence for short-range magnetic order in the nematic phase of FeSe, as has been suggested in several theoretical works [21–23].

II. EXPERIMENTAL METHODS

A. Sample growth and sample quality

Vapor-grown single crystals of FeSe [5,15,34], with typical dimensions of roughly 2 mm × 2 mm × (0.06–0.2) mm, were selected for this study. Figure 1 shows the resistivity and specific heat of a typical FeSe sample used in the magnetostriction and magnetization measurements. The discontinuous jump in the specific-heat data implies that the bulk superconducting transition occurs at $T_c = 9.1$ K [Fig. 1(a)]. It is the same temperature below which the resistivity becomes zero as shown in Fig. 1(b). The residual resistivity ratio (RRR) is estimated based on a linear extrapolation of the normal-state resistivity to zero temperature, and we obtain $RRR = R(300\text{ K})/R(0\text{ K}) \sim 166$. The large values of T_c and RRR prove that our samples are of high quality.

*christoph.meingast@kit.edu

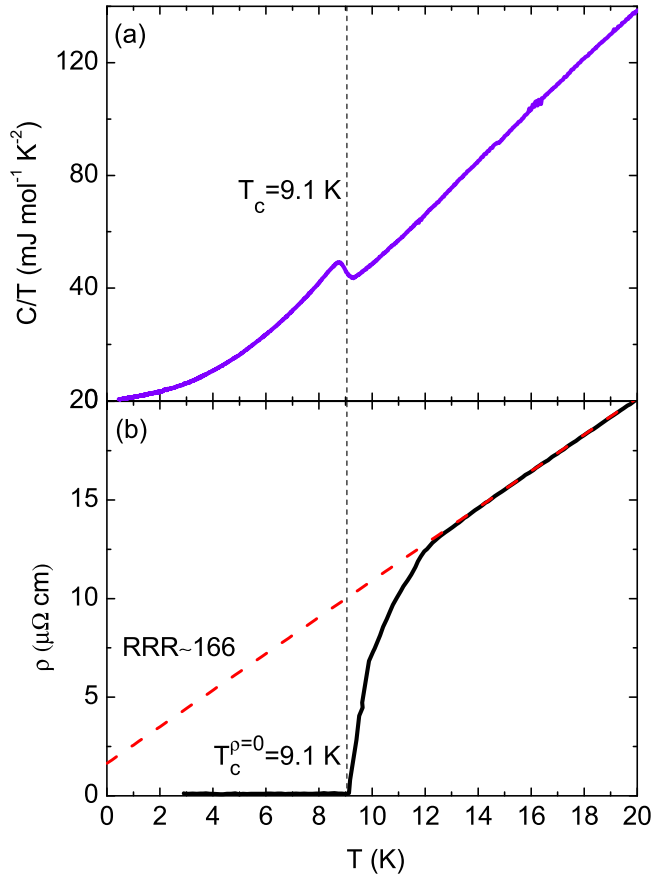


FIG. 1. Temperature dependence of the (a) specific heat and (b) resistivity in the vicinity of the superconducting transition. Both data show that $T_c = 9.1$ K. Red dashed line in (b) is an extrapolation according to a linear fit of the resistivity from 15 to 30 K, which gives the residual resistivity ratio $RRR = R(300 \text{ K})/R(0 \text{ K}) \sim 166$.

B. Detwinning setup

Resistivity anisotropy measurements using the glass-fiber-reinforced plastic (GFRP) substrate method, which was previously successfully employed for anisotropically straining BaFe_2As_2 [33], proved to be ineffective for applying a large strain to FeSe, i.e., no significant resistivity anisotropy could be observed. Most likely the crystals exfoliate due to the weak interlayer bonding using this method, and the top layer with the electrical contacts remains unstrained. We therefore used a “gentler” detwinning method incorporating General Electric 703 varnish (GE), which is schematically shown in Fig. 2(a) together with the electrical contacts for resistivity measurements. The single crystals were glued on top of a polyether ether ketone (PEEK) substrate by fixing two $[110]_t$ ends with GE varnish. For the magnetization measurements, a home-made PEEK sample holder was used, which has negligible magnetic response. Figure 2(b) shows the temperature dependence of the thermal expansion of the PEEK substrate and a free-standing FeSe sample along the two orthorhombic axes ($a > b$). The PEEK material has a much larger thermal-expansion coefficient than FeSe (along the a axis) and thus exerts a positive uniaxial strain on FeSe upon cooling. As a

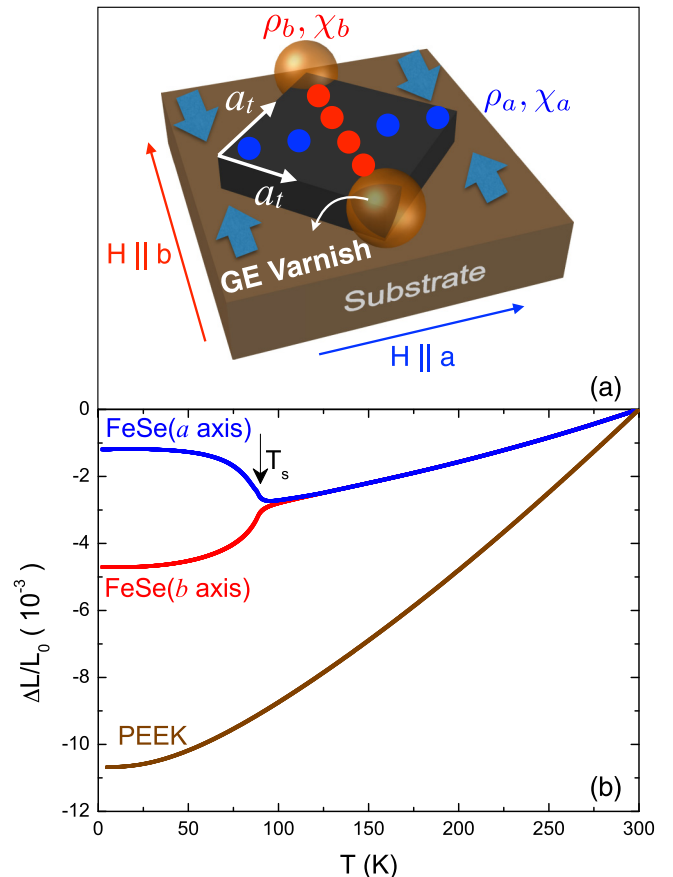


FIG. 2. (a) Schematic model of the uniaxial detwinning device. Blue and red dots are the electrical contacts for resistivity measurements along a and b axes respectively. (b) Thermal expansion of the PEEK substrate in comparison with a free-standing FeSe sample along orthorhombic a and b axes.

result, clear anisotropies in both resistivity and magnetization could be observed using this uniaxial-straining method.

C. Thermal-expansion and magnetostriction measurements

Thermal-expansion and magnetostriction measurements were made using a home-built high-resolution capacitance dilatometer [35].

D. Resistivity and magnetization experiments

Resistivity measurements were made using a standard four-terminal geometry [see Fig. 2(a)]. Magnetization measurements were carried out in a physical property measurement system (PPMS) using the vibrating sample magnetometer (VSM) from Quantum Design.

III. RESULTS

A. In-plane magnetostriction anisotropy of BaFe_2As_2 and FeSe

It has previously been shown that a high magnetic field applied along the $[110]_{\text{tet}}$ direction of the original tetragonal cell can be used to detwin BaFe_2As_2 crystals [36–38]. This field detwinning was attributed to an in-plane anisotropy of the magnetic susceptibility in the magnetically ordered state

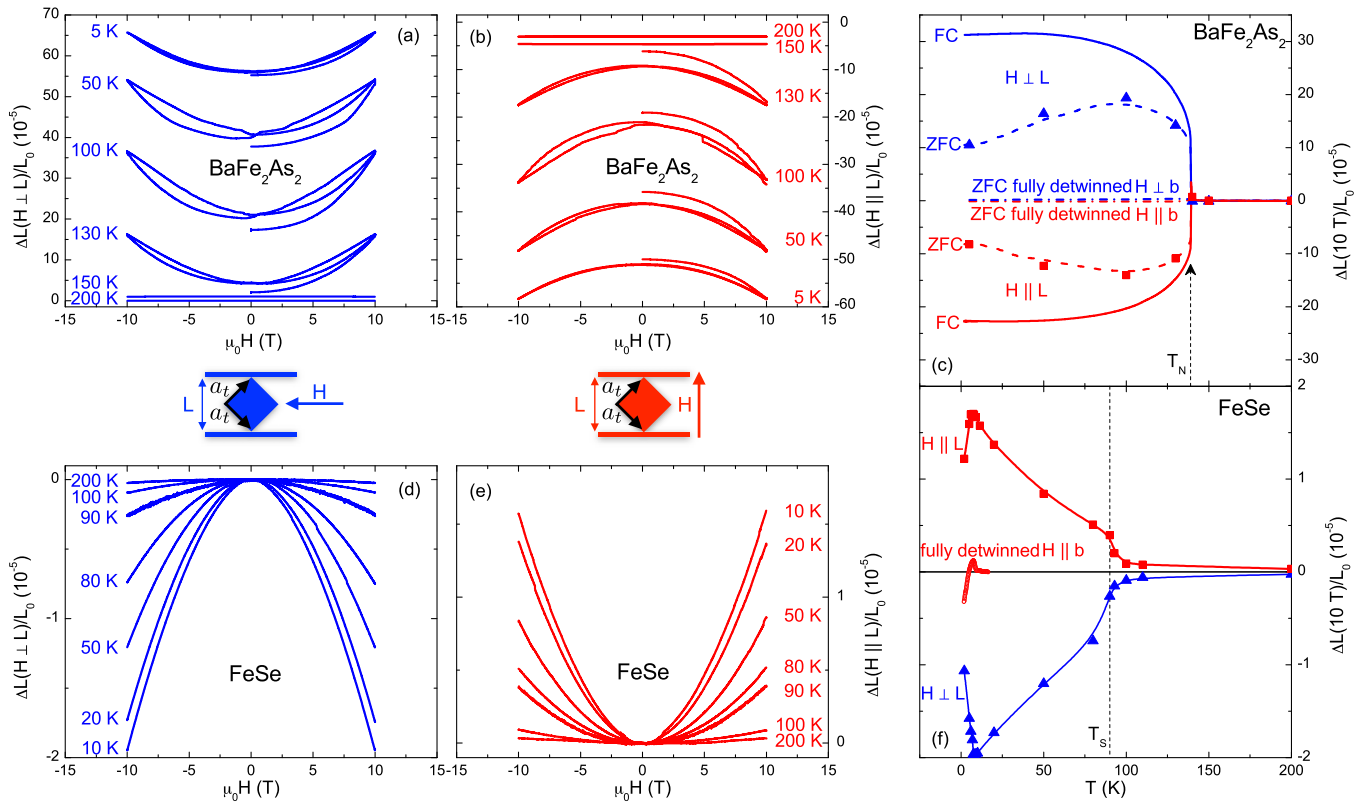


FIG. 3. Magnetostriction along the $[110]_{\text{tet}}$ direction of Ba122 (a),(b) and FeSe (d),(e) “twinned” single crystals for magnetic fields applied parallel and perpendicular to the length $L(H, T)$, as indicated by the accompanying illustrations. Field-cooled (FC) and zero-field-cooled (ZFC) differences in length changes between 0 and 10 T, derived from thermal-expansion measurements for BaFe_2As_2 (c) and taken directly from (d),(e) for FeSe (f). As outlined in the text, a significant magnetostriction results from a field-induced change in twin population resulting from a magnetic anisotropy in the orthorhombic phase. This magnetostriction practically vanishes for fully detwinned crystals [see (c) and (f)].

below $T_{S,N}$ [36,37], and, due to the considerable orthorhombic distortion within each magnetic domain, high-resolution magnetostriction measurements are expected to provide a very sensitive method for studying this effect. To set the stage, we first present magnetostriction data on BaFe_2As_2 , which has long-range magnetic order, and we then compare these data to those of FeSe.

To study field-induced detwinning, one needs to use a thick BaFe_2As_2 single crystal, for which the small force applied by the dilatometer is not sufficient to detwin [39,40] the sample. The magnetostriction of such a “thick crystal” is shown in Figs. 3(a) and 3(b) for two different field orientations and for temperatures between 200 and 5 K. Significant magnetostriction is only observed below $T_{S,N} = 139$ K. For the configuration $H \perp L$, L increases with field, whereas L decreases with field for $H \parallel L$. All curves below $T_{S,N}$ exhibit a considerable hysteresis, which can be attributed to the pinning of domain walls. We also performed field-cooled (FC) and zero-field-cooled (ZFC) thermal-expansion measurements at 10 T, from which the magnetostriction at 10 T was determined by subtracting the zero-field data as shown in Fig. 3(c). These data clearly show that the field-induced detwinning process abruptly starts below T_N . The solid symbols in Fig. 3(c) are taken from Figs. 3(a) and 3(b) and match the ZFC data very well. For fully detwinned crystals the magnetostriction practically vanishes as shown by the dash-dotted lines in Fig. 3(c). This demonstrates that the observed magnetostric-

tion is due to field-induced detwinning and not due to an intrinsic magnetostriction of the stripe magnetic state. The sign of the magnetostriction suggest that the shorter b axis has the higher susceptibility, which is consistent with direct measurements [33]. Domains with the b axis aligned along the field direction expand in population to lower the energy; as a result, L decreases (increases) with field for $H \parallel L$ (for $H \perp L$) as shown in Figs. 3(a) and 3(b).

In order to probe the nematic state in FeSe, we performed the same magnetostriction measurements on a “thick twinned” FeSe crystal [see Figs. 3(d)–3(f)]. The overall behavior is remarkably similar to that for BaFe_2As_2 ; i.e., the magnitude of the magnetostriction increases abruptly below T_S and is negligible above T_S . Similarly, for a “thin” fully detwinned sample, this magnetostriction signal vanishes [see Fig. 3(f)]. There are however also several important differences. First, the sign of the magnetostriction of FeSe is opposite that of BaFe_2As_2 , and the magnitude is about ten times smaller. Further, the magnetostriction of FeSe is free of hysteresis at all temperatures and the temperature dependence is quite different, increasing continuously down to low temperature. The implications of these results will be discussed below. Here we note that, using the above data, we can estimate that roughly 30 and 100 T are needed to fully detwin BaFe_2As_2 and FeSe, respectively (see Appendix B for details), in good agreement with Ref. [37] for BaFe_2As_2 . Further, the magnetic field can be translated to a uniaxial pressure, and at these respective fields

we find a uniaxial pressure of about 10 MPa for BaFe_2As_2 and 15 MPa in FeSe , which also agrees well with typical pressures needed to detwin these crystals [41]. Finally, we note that there is a large change in the magnetostriction response below T_c [see Fig. 3(f)], which will be treated in detail in a separate paper.

B. In-plane uniform magnetic susceptibility and resistivity anisotropies of FeSe

Since our magnetostriction data only provide indirect evidence for the susceptibility anisotropy, we also made an effort to measure this anisotropy directly by applying a uniaxial strain using the differential thermal expansion between FeSe and a PEEK sample holder, as described in the Methods section. We estimate (see Appendix A) that at the structural transition a strain of about 1×10^{-3} (approximately 30% of the spontaneous distortion) can be expected, which is sufficient to observe the in-plane anisotropy of the magnetic susceptibility, but which is not sufficient to exfoliate the crystal.

Figure 4(a) displays the resulting a - and b -axis magnetic susceptibilities, for $H = 12$ T, together with the twinned measurement. No background subtraction is needed in these measurements here, since the long weakly magnetic PEEK sample holder has essentially no signal in the VSM magnetometer. Above T_S , no difference between χ_a and χ_b can be resolved and the susceptibility scales linearly with temperature, as also observed in iron pnictides [33,42–44]. A kink around 90 K in both directions signals the nematic/structural transition, below which a clear splitting between χ_a and χ_b becomes evident. We find that the susceptibility measured along the shorter b axis is smaller than that of the a axis. This anisotropy is seen more clearly in the lower right inset of Fig. 4(a), in which the difference $\Delta\chi = \chi_b - \chi_a$ is plotted. The susceptibility anisotropy grows continuously from 0 above T_S to low temperature. Our results are quite similar to those of BaFe_2As_2 [33] in the sense that the anisotropy only develops below T_S . Interestingly, we however find $\chi_b < \chi_a$ for FeSe which is opposite in sign to that of BaFe_2As_2 , for which $\chi_b > \chi_a$ within the stripe anti-ferromagnetic (AF) phase [33]. This sign reversal also applies for the resistivity anisotropy, which we also measured using strain applied from a PEEK substrate (see Fig. 5). The sign of the resistivity anisotropy agrees with previous studies [6,29], however its magnitude varies greatly between the different measurements, which we attribute to the intrinsic difficulty of applying a well defined strain to FeSe . We note that an anisotropy of the Knight shift starting slightly above T_S in twinned crystals has also been observed in NMR measurements, however the sign of the anisotropy could not be determined due to the twinned nature of the crystals [15–17].

IV. DISCUSSION

We now discuss the implication of our experimental results. In Fig. 5 we compare the in-plane susceptibility and resistivity anisotropies of FeSe and BaFe_2As_2 [33]. Except for the opposite signs and different magnitudes of both effects, we find very similar behavior in both systems. Whereas the resistivity anisotropy develops well above and diverges upon

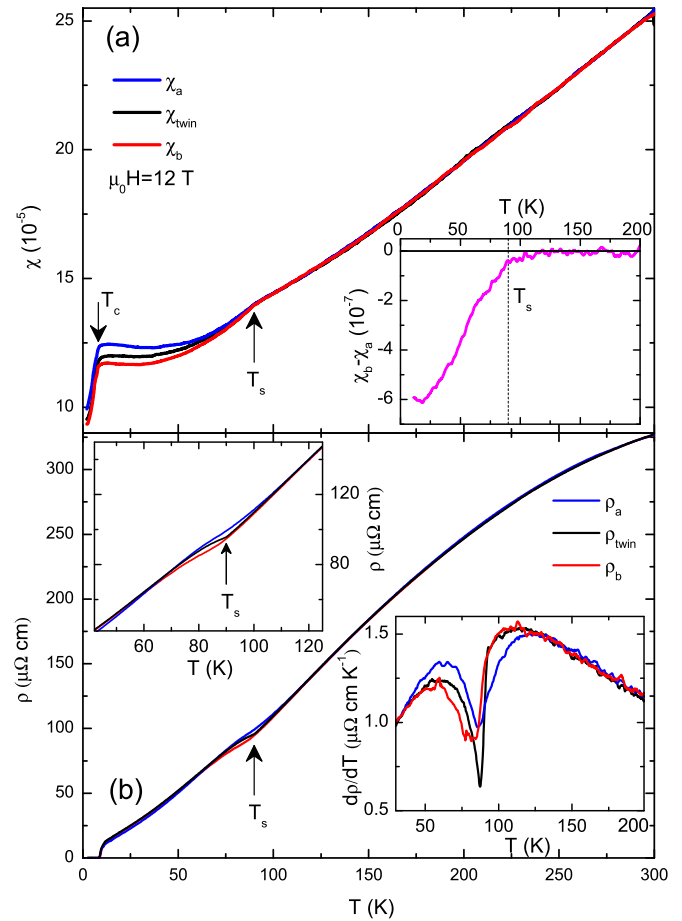


FIG. 4. (a) Temperature dependence of in-plane susceptibility anisotropy of FeSe in a field of 12 T. The crystal was detwinned using the thermally induced strain from the PEEK substrate sample holder [see Fig. 2(a) and text]. The black line is the susceptibility in the twinned state, taken on the same crystal. The inset on the lower right shows that the in-plane susceptibility anisotropy $\chi_b - \chi_a$ develops below T_S . (b) Resistivity anisotropy of FeSe measured using the same uniaxial strain setup as for the susceptibility measurements. A clear anisotropy is observed close to T_S (see inset in upper left). The inset in lower right presents the temperature derivative of the resistivity, which indicates that the structural transition is broadened under strain.

approaching T_S or T_N from above, the susceptibility anisotropy only appears below T_S or T_N . It was previously demonstrated that orbital order alone is insufficient to produce a sizable susceptibility anisotropy and that magnetic order and spin-orbit coupling are essential [33]. Using this same reasoning, we argue here that our data therefore provide strong evidence for some kind of magnetic order also in FeSe . Since there exists no evidence for long-range magnetic order in FeSe , likely candidates for magnetism are short-range frustrated magnetic orders in the nematic phase of FeSe , as suggested in several theoretical works [21–23]. We note that the proposed frustrated orders of Ref. [23] locally have a very similar ordering as in the long-ranged ordered stripe phase, forming a kind of phase-disordered AF chains. In a local picture, even such a short-range order is expected to result in a susceptibility anisotropy, albeit with a significantly reduced magnitude.

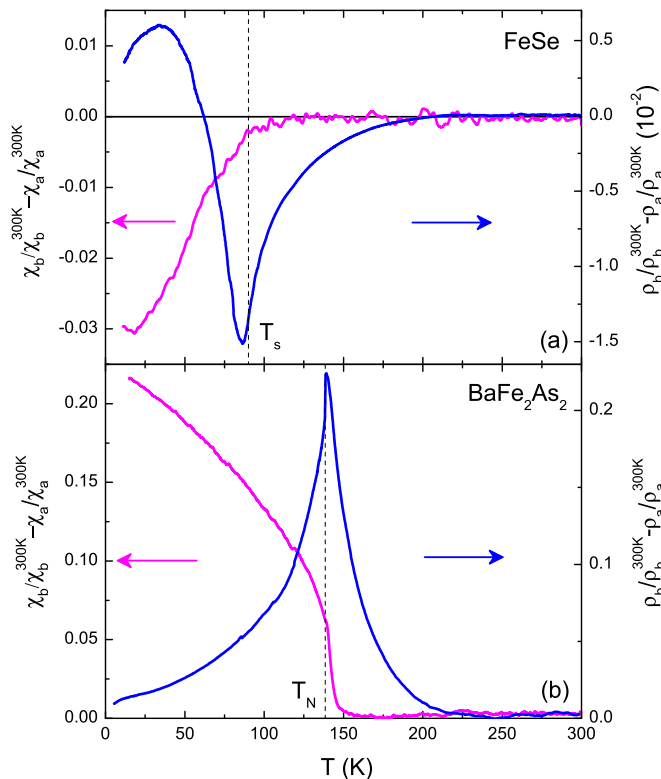


FIG. 5. Comparison of the susceptibility and resistivity anisotropies of (a) FeSe and (b) BaFe₂As₂. The data of BaFe₂As₂ are taken from Ref. [33]. Except for the magnitude and sign, the behavior of both systems is quite similar.

The opposite sign of the susceptibility of FeSe (compared to BaFe₂As₂) suggests that the spins, on average, are aligned along the shorter orthorhombic axis [33], in contrast to BaFe₂As₂.

Finally, in Fig. 6, we compare the temperature dependence of the field-induced distortion $\Delta\delta_H$ to the zero-field spontaneous distortion δ_T , inferred from our thermal-expansion data. For BaFe₂As₂, both quantities have similar temperature dependencies suggesting an intimate connection between the magnetic order and structural distortion. In fact, $\Delta\delta_H$ scales perfectly with δ_T^2 [see inset of Fig. 6(b)], which may provide important details about the magnetostrictive coupling in this material [45]. In contrast to BaFe₂As₂, there is no clear relation between these quantities for FeSe. Instead of flattening at low T , $\Delta\delta_H$ of FeSe continues to increase down to T_c . This suggests that either the strength or the nature of the magnetic short-range order in FeSe is strongly temperature dependent, which is consistent with the frustrated scenario. Indeed, similar to the susceptibility anisotropy, the spin-relaxation rate in FeSe also only emerges below T_S and diverges at low temperature before T_c is approached [15–17]. Our findings therefore point to a strong involvement of the spin degrees of freedom in the nematic transition of FeSe. The suggested frustrated magnetic ground state in FeSe is moreover strongly supported by the observation of both stripe- and Néel-type spin fluctuations in recent inelastic neutron-scattering (INS) experiments, in which the stripe-type magnetic signal becomes stronger below the nematic phase transition [24–26]. A more direct test for the

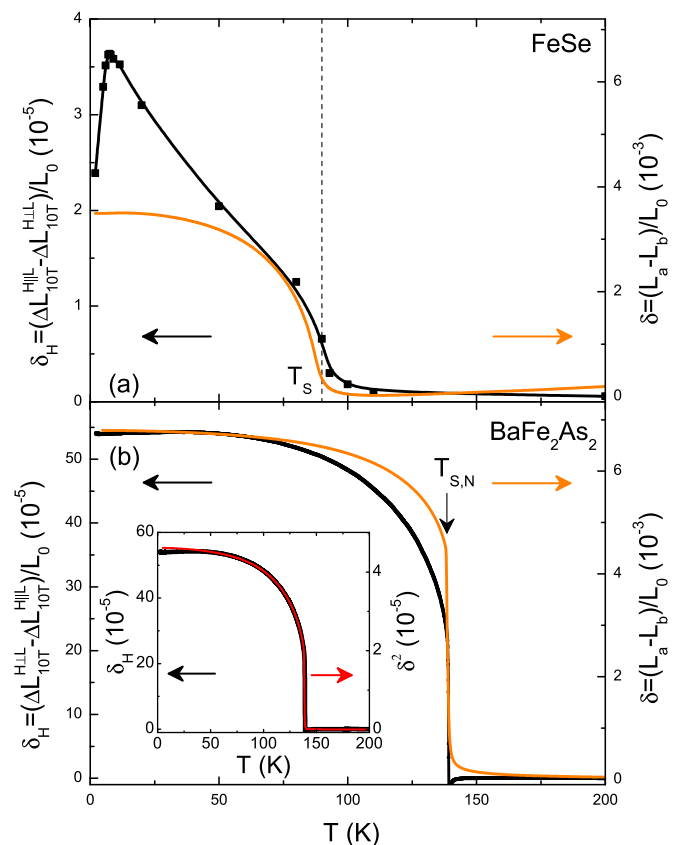


FIG. 6. Attempted scaling of the field-induced distortion at 10 T, $\Delta\delta_H$, with the spontaneous orthorhombic distortion δ_T , for (a) FeSe and (b) BaFe₂As₂. Whereas a rough scaling is observed for BaFe₂As₂, this scaling does not work for FeSe. In particular, $\Delta\delta_H$ of FeSe continues to increase to lower temperatures, whereas δ_T becomes flat. The inset in (b) shows that nearly perfect scaling can be obtained for BaFe₂As₂ if one scales $\Delta\delta_H$ with δ_T^2 .

involvement of magnetism in the nematic phase would involve neutron measurements on detwinned crystals, in which one would search for an imbalance of fluctuations with ordering vectors $\mathbf{Q}_1 = (\pi, 0)$ or $\mathbf{Q}_2 = (0, \pi)$.

V. CONCLUSIONS

In summary, the nematic phase of FeSe has been studied using measurements of the in-plane anisotropies of the uniform magnetic susceptibility, the magnetostriction, and the resistivity. Similar to BaFe₂As₂, the susceptibility and magnetostriction anisotropies develop only below the nematic transition temperature, whereas the resistivity anisotropy starts to develop at much higher temperatures. The sizable susceptibility anisotropy in these systems is due to spin-orbit coupling and develops only in the presence of magnetic order [33]. Our results thus strongly support the existence of some kind of short-range magnetic order within the nematic phase of FeSe and suggest that nematicity in iron-based systems is universally induced by magnetism. Neutron-scattering experiments on detwinned FeSe crystals are needed to directly clarify the nature of this proposed short-range magnetic order.

ACKNOWLEDGMENT

We thank I. Eremin, I. Mazin, and Q. Si for valuable discussions.

M.H. and L.W. contributed equally to this work.

APPENDIX A: STRAIN ESTIMATION

In order to estimate the uniaxial strain applied to the FeSe crystal in our detwinning method, we compare the measured in-plane resistivity anisotropy and the corresponding elastoresistivity with that obtained by piezoelectric stack measurements [29]. Using the resistivity data shown in Fig. 4(b), we adjust the strain to match the m_{66} channel of the elastoresistivity probed by piezoelectric stack measurements [29]:

$$2m_{66}(T) = \frac{\rho_b(T) - \rho_a(T)}{\rho_T(T)[\varepsilon_b(T) - \varepsilon_a(T)]}, \quad (\text{A1})$$

$$\varepsilon_b(T) - \varepsilon_a(T) = \varepsilon_b(T)(1 + \nu), \quad (\text{A2})$$

$$\varepsilon_b(T) \approx \gamma[\Delta L_{PEEK}/L_0 - \Delta L_{FeSe}^{twin}/L_0], \quad (\text{A3})$$

where ν is the Poisson ratio of FeSe extracted from ultrasound experiments [46], and $\gamma \sim 5\%$ is the strain transmission coefficient which is estimated by scaling our data with the $2m_{66}$ obtained by piezoelectric stack measurements [29]. The calculated $2m_{66}$ are presented in Fig. 7(a) and the same convention of $-2m_{66}$ is plotted in order to compare with BaFe₂As₂. The obtained $2m_{66}$ scales excellently with piezoelectric stack experiments above the transition, which exhibits a divergent Curie-Weiss behavior approaching T_S from above. An unusual sign change occurs at $T^* = 62$ K which is higher than that observed by Tanatar *et al.* [29] but agrees quite well with that found by Watson *et al.* [6], which has been attributed to strong anisotropic scattering in the orthorhombic phase [6]. We note that the magnitude of $|2m_{66}|$ at low temperature is relatively larger than that measured by Tanatar *et al.* [29]. This is possibly due to the extremely small residual resistivity ρ_T at low temperature [see Fig. 1(b)] which is used in the denominator of Eq. (A1). The estimated strain $\varepsilon_a(T) - \varepsilon_b(T)$ is plotted in Fig. 7(b) together with the sample lattice distortion, which gives a strain of $\sim 1 \times 10^{-3}$ ($\sim 30\%$ of the spontaneous lattice distortion) at T_S .

APPENDIX B: FIELD-INDUCED DETWINNING

As shown in Fig. 3, applying a magnetic field along the $[110]_{\text{tet}}$ direction effectively detwins the sample. Hence, a magnetic field acts equivalently to uniaxial pressure, which is commonly used in conventional detwinning devices. From the magnetostriction data $\Delta L_i(H)/L_0$, we can estimate the magnetic field and the corresponding pressure necessary to fully detwin BaFe₂As₂ and FeSe. The field-induced length change, $\Delta L_i(H)/L_0$, is related to the uniaxial pressure dependence of the magnetic susceptibility, $\frac{d\chi_i}{dp_i}$, according to a thermodynamic Maxwell equation:

$$\lambda = \frac{1}{\mu_0 V} \frac{\partial V}{\partial H} \Big|_{P,T} = -\frac{1}{V} \frac{\partial M}{\partial p} \Big|_{T,H} = -\frac{1}{V} \frac{\partial \chi}{\partial p} H, \quad (\text{B1})$$

$$\Delta L_i(H)/L_0 = -\left(\frac{\partial \chi_i}{\partial p_i}\right) \mu_0 H^2.$$

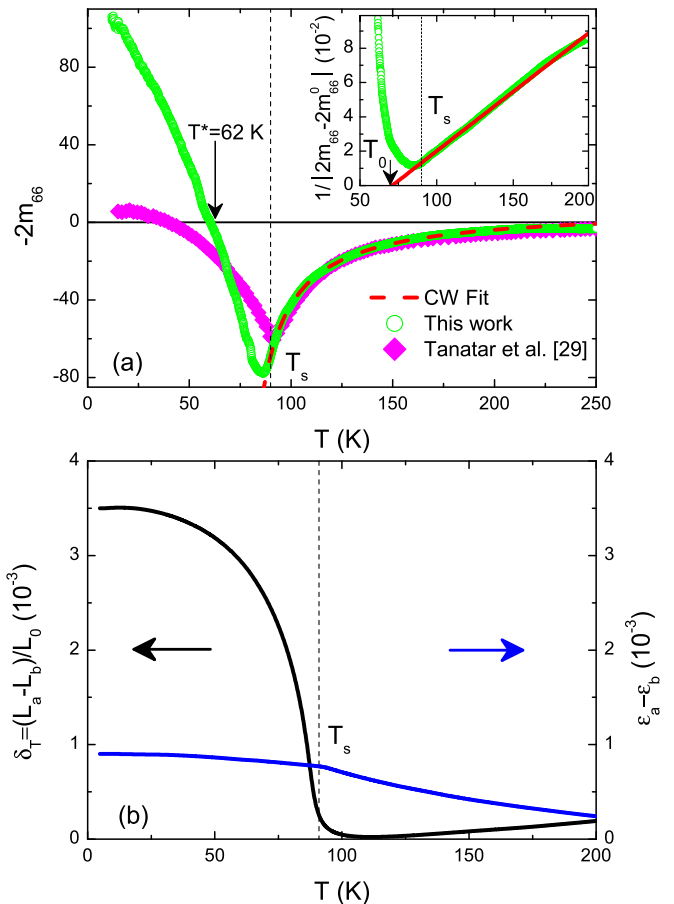


FIG. 7. (a) Calculated elastoresistivity coefficient $-2m_{66}$ (green circles) scaled with that measured by piezoelectric stack experiments (magenta squares) [29]. The red dashed line is the Curie-Weiss fitting in the form of $-2m_{66} = -2m_{66}^0 - a/(T - T_0)$ with $T_0 = 71 \pm 0.5$ K (inset: inverse version of Curie-Weiss fitting). (b) Temperature dependence of the estimated strain $\varepsilon_a(T) - \varepsilon_b(T)$ experienced by the sample in comparison with the lattice distortion δ_T of a free-standing FeSe sample.

The quadratic behavior $\Delta L_i(H)/L_0 = c_i H^2$ is evident in the data shown in Fig. 3. Therefore the field-induced distortion is also quadratic as a function of magnetic field

$$\Delta \delta_H = (\Delta L_H^{H \perp L} - \Delta L_H^{H \parallel L})/L_0 = \kappa H^2, \quad (\text{B2})$$

where κ is a constant. Since the field induced distortion $\Delta \delta_H$ at a field of 10 T is $\sim 10\%$ and $\sim 1\%$ of the spontaneous lattice distortion δ_T in BaFe₂As₂ and FeSe, respectively (see Fig. 6), the field H_{detwin} needed to fully detwin the sample is given by

$$H_{\text{detwin}} = \sqrt{\frac{\delta_T}{\Delta \delta_{H=10T}}} \times 10 \text{ T}. \quad (\text{B3})$$

We obtain $H_{\text{detwin}} \sim 30$ T for BaFe₂As₂ which agrees excellently with earlier reports [36,37]. For FeSe, the much larger field $H_{\text{detwin}} \sim 100$ T is necessary because the susceptibility anisotropy is fairly weak.

In the twinned state, the system's susceptibility is an average along both directions, i.e., $\chi_0(H, P = 0) = \frac{\chi_b + \chi_a}{2}$. For BaFe₂As₂, the susceptibility changes to $\chi_{\text{detwin}} = \chi_b$ in the

fully detwinned state with one single domain when H_{detwin} is reached, in which the shorter b axis aligns along the field direction. Then the effective pressure required to fully detwin BaFe_2As_2 is obtained:

$$\chi_{\text{detwin}} - \chi_0 = (P_{\text{detwin}} - 0) \frac{d\chi}{dp} \quad (\text{B4})$$

$$\Rightarrow P_{\text{detwin}} = \frac{(\chi_b - \chi_a)}{2d\chi/dp}. \quad (\text{B5})$$

From the magnetostriction data presented in the Fig. 3 and according to Eq. (B1), a uniaxial-pressure dependence of the magnetic susceptibility for BaFe_2As_2 of $\frac{d\chi}{dp} \sim 1.5 \times 10^{-6} \text{ MPa}^{-1}$ is obtained at 100 K. The susceptibility

anisotropy of BaFe_2As_2 at 100 K is $\chi_b - \chi_a \sim 3 \times 10^{-5}$ [33], and we find $P_{\text{detwin}} \sim 10 \text{ MPa}$ at 100 K, which matches the value obtained by applying uniaxial pressure directly [41] quite well. Similarly, for FeSe , $\frac{d\chi}{dp} \sim 2.5 \times 10^{-7} \text{ MPa}^{-1}$ and $\chi_a - \chi_b \sim 7.5 \times 10^{-6}$ at 10 K [see Fig. 4(a)], hence $P_{\text{detwin}} \sim 15 \text{ MPa}$.

The effective field induced pressure at 10 T can also be estimated,

$$P_{H=10\text{T}} = \frac{10\text{T}}{H_{\text{detwin}}} P_{\text{detwin}}. \quad (\text{B6})$$

For BaFe_2As_2 , $H_{\text{detwin}} \sim 30 \text{ T}$ and $P_{\text{detwin}} \sim 10 \text{ MPa}$, hence we have $P_{H=10\text{T}} \sim 10 \text{ T}/30 \text{ T} \cdot 10 \text{ MPa} \sim 3 \text{ MPa}$. For FeSe , $H_{\text{detwin}} \sim 100 \text{ T}$ and $P_{\text{detwin}} \sim 15 \text{ MPa}$, therefore one gets $P_{H=10\text{T}} \sim 10 \text{ T}/100 \text{ T} \times 15 \text{ MPa} \sim 1.5 \text{ MPa}$.

-
- [1] P. J. Hirschfeld, M. M. Korshunov, and I. I. Mazin, *Rep. Prog. Phys.* **74**, 124508 (2011).
- [2] A. Chubukov, *Annu. Rev. Condens. Matter Phys.* **3**, 57 (2012).
- [3] F.-C. Hsu, J.-Y. Luo, K.-W. Yeh, T.-K. Chen, T.-W. Huang, P. M. Wu, Y.-C. Lee, Y.-L. Huang, Y.-Y. Chu, D.-C. Yan, and M.-K. Wu, *Proc. Natl. Acad. Sci. USA* **105**, 14262 (2008).
- [4] T. M. McQueen, A. J. Williams, P. W. Stephens, J. Tao, Y. Zhu, V. Ksenofontov, F. Casper, C. Felser, and R. J. Cava, *Phys. Rev. Lett.* **103**, 057002 (2009).
- [5] A. E. Böhmer, F. Hardy, F. Eilers, D. Ernst, P. Adelmann, P. Schweiss, T. Wolf, and C. Meingast, *Phys. Rev. B* **87**, 180505 (2013).
- [6] M. D. Watson, T. K. Kim, A. A. Haghighirad, N. R. Davies, A. McCollam, A. Narayanan, S. F. Blake, Y. L. Chen, S. Ghannadzadeh, A. J. Schofield, M. Hoesch, C. Meingast, T. Wolf, and A. I. Coldea, *Phys. Rev. B* **91**, 155106 (2015).
- [7] C. Fang, H. Yao, W.-F. Tsai, J. P. Hu, and S. A. Kivelson, *Phys. Rev. B* **77**, 224509 (2008).
- [8] S. Nandi, M. G. Kim, A. Kreyssig, R. M. Fernandes, D. K. Pratt, A. Thaler, N. Ni, S. L. Bud'ko, P. C. Canfield, J. Schmalian, R. J. McQueeney, and A. I. Goldman, *Phys. Rev. Lett.* **104**, 057006 (2010).
- [9] R. M. Fernandes and J. Schmalian, *Supercond. Sci. Technol.* **25**, 084005 (2012).
- [10] R. M. Fernandes, A. V. Chubukov, and J. Schmalian, *Nat. Phys.* **10**, 97 (2014).
- [11] F. Krüger, S. Kumar, J. Zaanen, and J. van den Brink, *Phys. Rev. B* **79**, 054504 (2009).
- [12] H. Kontani and S. Onari, *Phys. Rev. Lett.* **104**, 157001 (2010).
- [13] H. Kontani, T. Saito, and S. Onari, *Phys. Rev. B* **84**, 024528 (2011).
- [14] H. Yamase and R. Zeyher, *Phys. Rev. B* **88**, 180502 (2013).
- [15] A. E. Böhmer, T. Arai, F. Hardy, T. Hattori, T. Iye, T. Wolf, H. v. Löhneysen, K. Ishida, and C. Meingast, *Phys. Rev. Lett.* **114**, 027001 (2015).
- [16] S.-H. Baek, D. V. Efremov, J. M. Ok, J. S. Kim, J. van den Brink, and B. Büchner, *Nat. Mater.* **14**, 210 (2015).
- [17] S.-H. Baek, D. V. Efremov, J. M. Ok, J. S. Kim, J. van den Brink, and B. Büchner, *Phys. Rev. B* **93**, 180502 (2016).
- [18] A. Kreisel, S. Mukherjee, P. J. Hirschfeld, and B. M. Andersen, *Phys. Rev. B* **92**, 224515 (2015).
- [19] S. Mukherjee, A. Kreisel, P. J. Hirschfeld, and B. M. Andersen, *Phys. Rev. Lett.* **115**, 026402 (2015).
- [20] Y. Yamakawa, S. Onari, and H. Kontani, *Phys. Rev. X* **6**, 021032 (2016).
- [21] R. Yu and Q. Si, *Phys. Rev. Lett.* **115**, 116401 (2015).
- [22] F. Wang, S. A. Kivelson, and D.-H. Lee, *Nat. Phys.* **11**, 959 (2015).
- [23] J. K. Glasbrenner, I. I. Mazin, H. O. Jeschke, P. J. Hirschfeld, R. M. Fernandes, and R. Valenti, *Nat. Phys.* **11**, 953 (2015).
- [24] M. C. Rahn, R. A. Ewings, S. J. Sedlmaier, S. J. Clarke, and A. T. Boothroyd, *Phys. Rev. B* **91**, 180501 (2015).
- [25] Q. Wang, Y. Shen, B. Pan, Y. Hao, M. Ma, F. Zhou, P. Steffens, K. Schmalzl, T. R. Forrest, M. Abdel-Hafiez, X. Chen, D. A. Chareev, A. N. Vasiliev, P. Bourges, Y. Sidis, H. Cao, and J. Zhao, *Nat. Mater.* **15**, 159 (2016).
- [26] Q. Wang, Y. Shen, B. Pan, X. Zhang, K. Ikeuchi, K. Iida, A. D. Christianson, H. C. Walker, D. T. Adroja, M. Abdel-Hafiez, X. Chen, D. A. Chareev, A. N. Vasiliev, and J. Zhao, *Nat. Commun.* **7**, 12182 (2016).
- [27] A. E. Böhmer and C. Meingast, *C. R. Phys.* **17**, 90 (2016).
- [28] A. E. Böhmer and A. Kreisel, *J. Phys.: Condens. Matter* **30**, 023001 (2018).
- [29] M. A. Tanatar, A. E. Böhmer, E. I. Timmons, M. Schütt, G. Drachuck, V. Taufour, K. Kothapalli, A. Kreyssig, S. L. Bud'ko, P. C. Canfield, R. M. Fernandes, and R. Prozorov, *Phys. Rev. Lett.* **117**, 127001 (2016).
- [30] M. Ma, P. Bourges, Y. Sidis, Y. Xu, S. Li, B. Hu, J. Li, F. Wang, and Y. Li, *Phys. Rev. X* **7**, 021025 (2017).
- [31] P. Massat, D. Farina, I. Paul, S. Karlsson, P. Strobel, P. Toulemonde, M.-A. Méasson, M. Cazayous, A. Sacuto, S. Kasahara, T. Shibauchi, Y. Matsuda, and Y. Gallais, *Proc. Natl. Acad. Sci. USA* **113**, 9177 (2016).
- [32] A. Baum, H. N. Ruiz, N. Lazarević, Y. Wang, T. Böhm, R. H. Ahangharnejhad, P. Adelmann, T. Wolf, Z. V. Popović, B. Moritz, T. P. Devereaux, and R. Hackl, [arXiv:1709.08998](https://arxiv.org/abs/1709.08998).
- [33] M. He, L. Wang, F. Ahn, F. Hardy, T. Wolf, P. Adelmann, J. Schmalian, I. Eremin, and C. Meingast, *Nat. Commun.* **8**, 504 (2017).
- [34] L. Wang, F. Hardy, T. Wolf, P. Adelmann, R. Fromknecht, P. Schweiss, and C. Meingast, *Phys. Status Solidi B* **254**, 1600153 (2016).

- [35] C. Meingast, B. Blank, H. Bürkle, B. Obst, T. Wolf, H. Wühl, V. Selvamanickam, and K. Salama, *Phys. Rev. B* **41**, 11299 (1990).
- [36] J.-H. Chu, J. G. Analytis, D. Press, K. De Greve, T. D. Ladd, Y. Yamamoto, and I. R. Fisher, *Phys. Rev. B* **81**, 214502 (2010).
- [37] J. P. C. Ruff, J.-H. Chu, H.-H. Kuo, R. K. Das, H. Nojiri, I. R. Fisher, and Z. Islam, *Phys. Rev. Lett.* **109**, 027004 (2012).
- [38] S. Zapf, C. Stingl, K. W. Post, J. Maiwald, N. Bach, I. Pietsch, D. Neubauer, A. Löhle, C. Clauss, S. Jiang, H. S. Jeevan, D. N. Basov, P. Gegenwart, and M. Dressel, *Phys. Rev. Lett.* **113**, 227001 (2014).
- [39] A. E. Böhmer, F. Hardy, L. Wang, T. Wolf, P. Schweiss, and C. Meingast, *Nat. Commun.* **6**, 7911 (2015).
- [40] L. Wang, F. Hardy, A. E. Böhmer, T. Wolf, P. Schweiss, and C. Meingast, *Phys. Rev. B* **93**, 014514 (2016).
- [41] H. Man, X. Lu, J. S. Chen, R. Zhang, W. Zhang, H. Luo, J. Kulda, A. Ivanov, T. Keller, E. Morosan, Q. Si, and P. Dai, *Phys. Rev. B* **92**, 134521 (2015).
- [42] X. F. Wang, T. Wu, G. Wu, H. Chen, Y. L. Xie, J. J. Ying, Y. J. Yan, R. H. Liu, and X. H. Chen, *Phys. Rev. Lett.* **102**, 117005 (2009).
- [43] G. M. Zhang, Y. H. Su, Z. Y. Lu, Z. Y. Weng, D. H. Lee, and T. Xiang, *Europhys. Lett.* **86**, 37006 (2009).
- [44] R. Klingeler, N. Leps, I. Hellmann, A. Popa, U. Stockert, C. Hess, V. Kataev, H.-J. Grafe, F. Hammerath, G. Lang, S. Wurmehl, G. Behr, L. Harnagea, S. Singh, and B. Büchner, *Phys. Rev. B* **81**, 024506 (2010).
- [45] C. J. Howard and M. A. Carpenter, *Acta Cryst. B* **68**, 209 (2012).
- [46] G. A. Zvyagina, T. N. Gaydamak, K. R. Zhekov, I. V. Bilich, V. D. Fil, D. A. Chareev, and A. N. Vasiliev, *Europhys. Lett.* **101**, 56005 (2013).